Prediction of Achievable Energy Deposition for Vaporizing Foil Actuators

M. Hahn[*1], S.R. Hansen[2], S. Gies[1], A. Vivek[2], G.S. Daehn[2], A.E. Tekkaya[1]

[1] Institute of Forming Technology and Lightweight Components, TU Dortmund University, Germany
[2] Department of Materials Science and Engineering, The Ohio State University, USA
*Corresponding author. Email: Marlon.Hahn@iul.tu-dortmund.de

Abstract

A novel iterative analytic approach allowing for the prediction of energy deposition into Vaporizing Foil Actuators (VFA) is presented. Besides the process parameters of actuator geometry and pulse generator configuration, it takes into account the energy dependence of the resistivity as well as the rate dependence of the achievable energy deposition. This rate dependency is found experimentally for aluminum foils and subsequently used in the modeling. With an average deviation of less than 15% the predicted energy depositions are in acceptable accordance with the experiments, but only as long as homogeneous Joule heating can be assumed. The proposed model has thus the potential to ease the future VFA process design, e.g. for manufacturing applications.

Keywords

Vaporizing Foil Actuator, Energy Deposition, Joule Heating, Analytical Model

1 Introduction

The electrical explosion of metal foils has recently gained attention in the field of manufacturing research in the form of so-called Vaporizing Foil Actuators (VFA). The electrical explosion phenomenon by itself has already been known for some decades from other contexts (mainly shock physics, see Weingart et al. (1976), for example). Since the utilization of VFA for manufacturing purposes is a rather novel approach, the underlying physics are explained briefly in the following paragraphs with respect to the fields of application in metalworking.

If a high current flows through a comparatively small conductor cross section (wire or foil actuators as elements of an RLC circuit, see **Fig. 1**), the conductor is heated up very rapidly, which leads to phase changes. As explained by Winkler (1973), thanks to inertial effects and Lorentz forces, the resistive energy deposition can cause temperature rises exceeding the boiling point of the material before the conductor disintegrates. After reaching the gaseous state, the resistivity becomes significantly larger than in the solid and liquid states, typically resulting in a distinct peak in the voltage history. At this point, the burst time t_B, the conductor abruptly expands in a high-pressure burst. From then on, conductivity cannot be preserved anymore, and the current drops. In some cases, a subsequent plasma restrike may occur.

If a workpiece is intentionally placed in close vicinity to the actuator, the expanding vapor can be used to generate high stresses in the workpiece that allow for plastic deformation. As shown in Vivek et al. (2013 a-b) and in **Fig. 1**, this enables application in four manufacturing fields for sheet metals or tubes: forming, joining, embossing, and cutting. Workpiece velocities in the range of 1 km/s can be reached (Hahn et al., 2016).

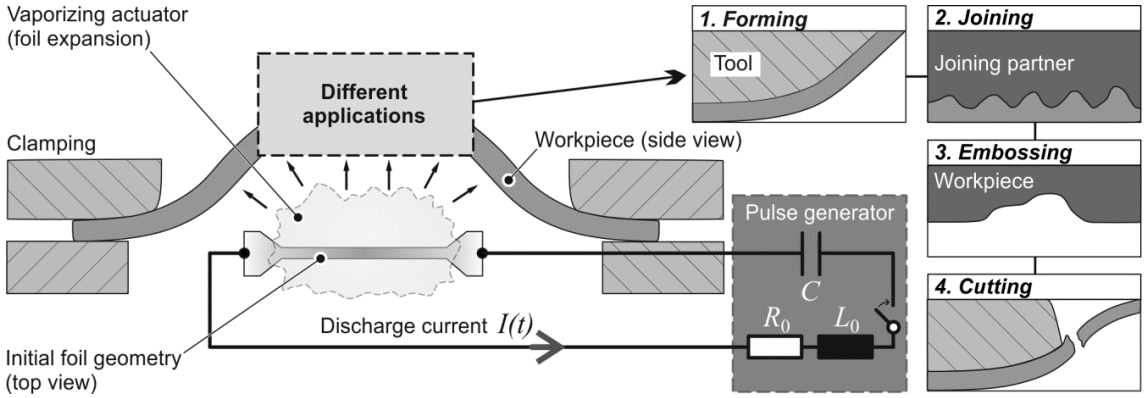

***Figure 1**: Basic principle of VFA and their applications in metalworking*

The question about the maximum possible amount of energy that can be deposited until t_B has been controversially discussed in literature. Sedoi et al. (1999) outlined that some authors claimed it to be a material constant, while others proved experimentally that it can be enhanced by increasing the (average) rate of Joule heating. Those authors also stated that the shape of the conductor cross section has no influence in this regard.

The specific energy deposition into the foil before t_B is a crucial variable governing the output pressure available for the forming of a workpiece, and is thus of fundamental interest for VFA process design. However, a predictive model providing the energy deposition at the burst time as a consequence of the chosen process parameters (foil actuator geometry and material; resistance, capacitance, inductance and charging energy of the pulse generator), could not be found in literature so far. It is the aim of this work to establish and validate such a model to facilitate future process design. It is therefore necessary that the model incorporates both the dependence of the resistivity of the actuator material on its current state of specific energy, and the rate dependence of the achievable energy deposition.

2 Experimental Determination of Energy Deposition

2.1 Experimental Configuration and Data Acquisition

To solely investigate the achievable deposition of electrical energy, the used setup did not contain a deformable workpiece. Instead, the foil was mechanically constrained through massive screwed steel backings and always well insulated with Kapton polyimide tape to prevent arcing between metal components. An image of the setup with a mounted exemplary foil before and after vaporization is given in **Fig. 2**.

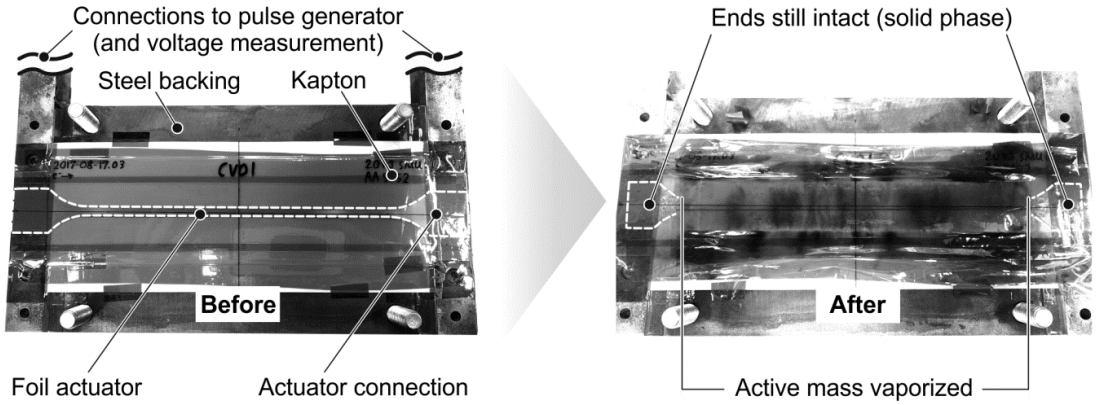

***Figure 2**: Experimental setup (opened) including actuator before and after vaporization*

The parameters varied were the resonance frequency $f_{res} = 1/\left(2\pi\sqrt{L_0 C}\right)$ of the capacitor bank (two pulse generators: "Magneform" from Maxwell Labs, 24 kHz; "SMU0612" from Poynting, 97 kHz), and the initial charging energy ($1.3\ \text{kJ} \leq E_0 \leq 8.8\ \text{kJ}$). In addition, the geometry of the rectangular "active" region (the central constricted area of the dogbone-shaped aluminum foil actuators – density $\gamma = 2.7\ \text{g/cm}^3$) was varied while keeping the volume constant at $V_a = 30.5\ \text{mm}^3$. The foil specimens were manufactured by water jet cutting in the following geometric dimensions: width *b*, 4.5-24 mm; thickness *s*, 0.0254-0.1016 mm; length *l*, 50-200 mm.

During each experiment, voltage-time traces $U_{Setup}(t)$ were recorded with a 1000:1 voltage divider, as well as current-time traces $I(t)$ with a Rogowski coil. Further data processing was performed with the help of a 1 GS/s oscilloscope and the Matlab software. Within this processing, the burst time t_B was found by means of the distinct voltage peak, and the specific deposited energy w was assumed to be distributed homogeneously throughout the active mass $m_a = \gamma V_a$. Experimentally achieved specific energy depositions and their average rates were hence determined as follows (inductive energy fractions are neglected here).

$$w = \frac{W}{m_a} = \frac{1}{\gamma V_a}\int_0^{t_B} U_{Setup}\, I dt \Rightarrow \dot{w} = \frac{w}{t_B} \tag{1}$$

2.2 Rate Dependence of Energy Deposition

The heating rates resulting from the parameter variations explained in section **2.1** and the corresponding energy ratios (specific energy for full vaporization of Al: w_s = 13.34 kJ/g, derived from Osher et al. (1989)) are compiled in **Fig. 3** to establish a phenomenological curve $w(\dot{\bar{w}})$ for aluminum. Sedoi et al. (1999) did this for Cu and Ni wires. The effects of individual process parameters are discussed in section **4**, together with associated modeling results.

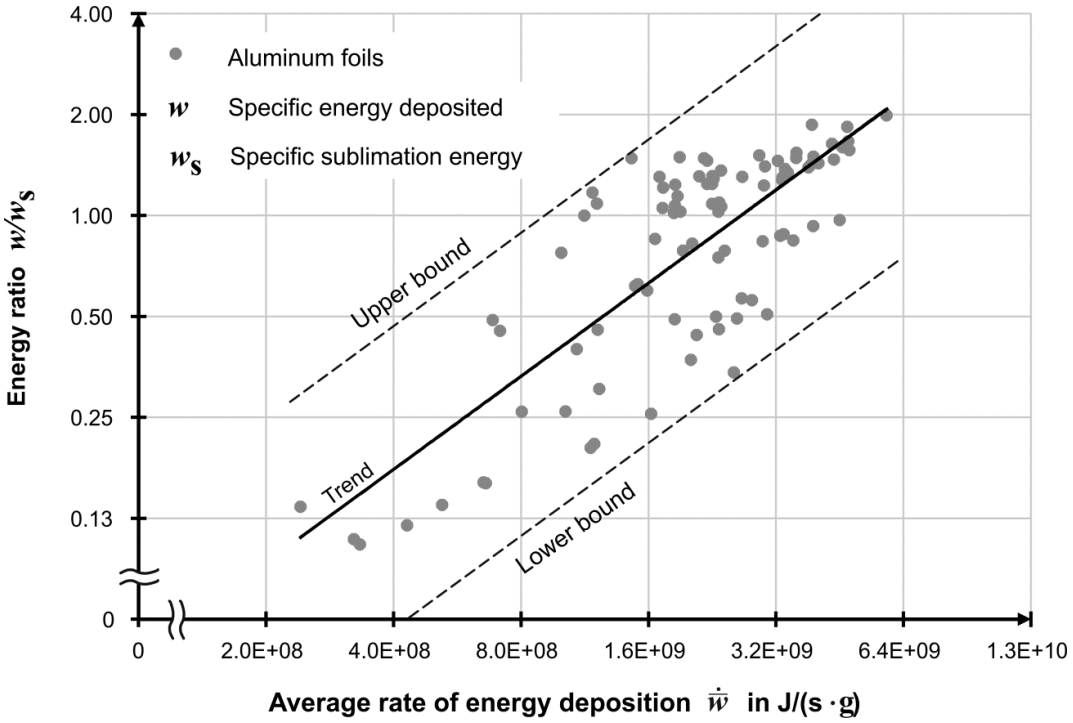

***Figure 3**: Experimental results for the rate dependence of energy deposition until t_B for Al*

Despite a large scattering, the general correlation addressed in the literature, $dw/d\dot{\bar{w}}$, can be recognized. The equation describing the trend line in **Fig. 3** is $w(\dot{\bar{w}}) \approx 2w_s\, 10^{-9}\dot{\bar{w}}^{0.923}$, covering a range of $3{\cdot}10^8$ J/(g·s) $\leq \dot{\bar{w}} \leq 6{\cdot}10^9$ J/(g·s) with $0.1 \leq w/w_s \leq 2$. Two possible reasons for the scattering can be given. First, **Eq. 1** just gives average values over time as well as over the total foil region to be vaporized. However, on a more detailed level, vaporization starts from the conductor surface, according to Tkachenko et al. (2004), meaning locally different points of the actual curve $w(\dot{\bar{w}})$ may be valid within one experiment. Such aspects can vanish when averaging over t_B and m_a. Second, of the peak current densities were in the range below which short-time magnetohydrodynamic (MHD) instabilities may occur, $j_{MHD} \approx (g - g_{melt}) \cdot \gamma^{-0.5}/12$ (taken from Sedoi et al. (1999) and anticipating **Eq. 5**). If those effects are pronounced, this could lead to a scatter in terms of energy depositions and heating rates calculated from **Eq. 1**.

3 Predictive Model for Energy Deposition

3.1 Governing Equations

The average heating rate $\dot{\bar{w}}$ is an important parameter for proper prediction of the energy deposition (**Fig. 3**). Key to estimating the heating rate resulting from chosen process parameters is the solving of the differential equation of the series RLC circuit of the actuator system. According to Al-Hassani et al. (1986), the general equation characterizing the transient current *I(t)* of such a system can be written as

$$L\ddot{I} + R\dot{I} + \left(\dot{R} + \frac{1}{C}\right) = 0. \tag{2}$$

R stands for the sum of the constant inner resistance of the pulse generator and the time-dependent resistance of the foil actuator, while *L* is the sum of the inductance of the pulse generator and the actuator. $L \approx$ const. applies, since it can be assumed that the geometry of the foil remains approximately constant until t_B (Zou et al., 2012). *C* is the capacitance of the pulse generator. To be able to find an analytical closed-form solution for **Eq. 2**, the simplification of using a constant average value $\bar{R}$ for the resistance *R* is made. When $R \approx \bar{R} = \text{const.}$ is presumed, $\dot{R} = 0$ applies, yielding

$$L\ddot{I} + \bar{R}\dot{I} + \frac{1}{C} = 0. \tag{3}$$

With charging energy E_0, the initial conditions to be postulated for **Eq. 3** are $I(t = 0) = 0$ and $U(t = 0) = L\dot{I}(t = 0) = \sqrt{2E_0/C}$, *U* being the voltage of the capacitor of the pulse generator. After the abovementioned simplification - depending on the concrete values of *L*, $\bar{R}$, and *C* - one out of three different standard solutions for *I(t)* can be found from basic electrical engineering literature: the underdamped case, the critically damped case, and the overdamped case. For the sake of brevity, those solutions are not shown here. Instead, focus is given to the part governing the resistive heating of the foil, as $\bar{R}$ is determined on this way. With resistivity ρ, current density *j*, and mass density γ, the achievable specific energy of the foil, *w*, can be expressed as

$$w = \int_0^{t_B} \frac{\rho}{\gamma} j^2 dt \tag{4}$$

where a homogeneous distribution of *j* over the conductor cross section *A* is assumed (uniform Joule heating: $j = I/A$). Keeping in mind that the foil geometry is believed to remain constant in the considered time regime, meaning γ = const. and *A* = const., the separation of variables yields the so-called action integral *g* (or *g*-value)

$$\gamma \int_0^w \frac{1}{\rho} dw = \int_0^{t_B} j^2 dt = g. \tag{5}$$

The average resistivity $\bar{\rho}$ until t_B is then given by

$$\bar{\rho} = \frac{w\gamma}{g} \tag{6}$$

wherein the material-specific relation $\rho(w)$, which effectively represents the temperature dependence of the resistivity, should be known. The average resistance of a foil segment n having length Δl_n, width b_n, and thickness s can be computed as

$$\bar{R}_n = \frac{\bar{\rho}_n \Delta l_n}{s b_n}. \tag{7}$$

If a foil actuator with a varying width along the direction of current flow is considered, it can be shown that the action integral for a foil segment of width b_k is related to another segment (index n) by

$$\frac{g_k}{g_n} = \left(\frac{b_n}{b_k}\right)^2. \tag{8}$$

This relation is useful for the spatial discretization of foil actuators, e.g. dogbone-shaped ones. The total resistance $\bar{R}$, which is included in **Eq. 3**, is finally determined by summing up the respective values for $\bar{R}_n$ of all sequential foil segments (plus R_0 as in **Fig. 1**).

3.2 Input Data and Solution Scheme

Regarding $\rho(w)$, a bi-linear approach is derived from data provided by Tucker and Toth (1975) for aluminum, as can also be seen in **Fig. 4**. For a linear region $\rho(w) = \rho_0 + \alpha w$ starting at a specific energy w_0, it follows that the action integral equates to

$$g(w) = \frac{\gamma}{\alpha} \ln\left(\frac{\rho_0 + \alpha w}{\rho_0 + \alpha w_0}\right) + g(w_0), \text{with } g(0) = 0. \tag{9}$$

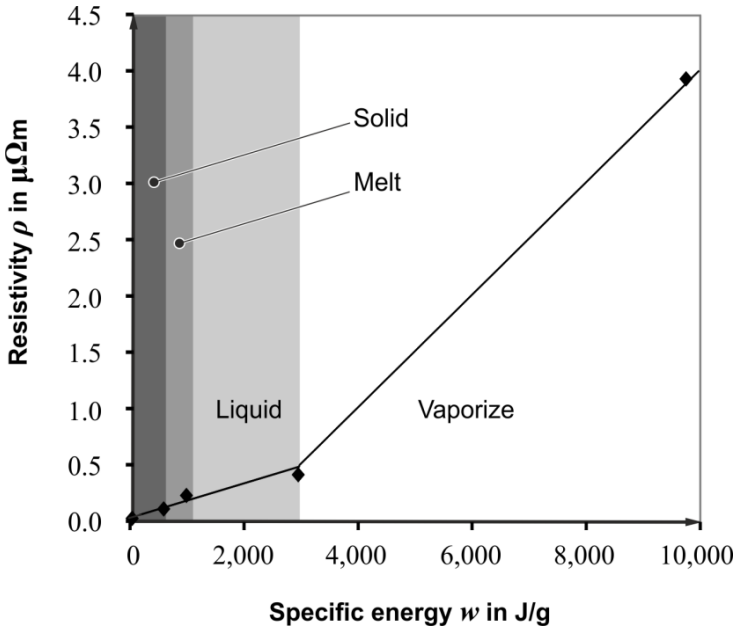

***Figure 4**: Resistivity versus specific energy for aluminum after Tucker and Toth (1975)*

For the rate dependency of the possible specific energy deposition, $w(\dot{\bar{w}})$, the experimentally obtained equation describing the trend line in **Fig. 3** is employed (as in section **2.2**). All geometric foil parameters, as well as all circuit parameters of the pulse generators, are taken from the experiments, as well. Foil inductances (discretized in rectangular segments) are calculated after standard formulas as, for instance, summarized in Kazimierczuk (2004).

A weak point of the proposed analytical model is that the final *g*-value (and thus a corresponding energy deposition as *w(g)* is known) actually needs to be known in advance when calculating the solution for the current density because $\bar{R}$ is a function of g for a given geometry (see section **3.1**). To overcome this problem, the model is applied iteratively until an initially required guess, g_{guess}, and an updated g, which results from the model, are identical (or rather if their difference is smaller than a certain percentage, e.g. 5% was chosen for the present work). This iterative procedure is illustrated in **Fig. 5**. With the transient solution for j based on g_{guess}, a theoretical burst time t_{B} can be determined by checking the subsequent condition.

$$g_{\text{guess}} = \int_0^{t_{\text{B}}} j^2 \, dt \Rightarrow t_{\text{B}} \tag{10}$$

From that, in turn, an underlying heating rate $\dot{\bar{w}}$ results, and so on (see **Fig. 5**). Experience shows that typically not more than five iteration loops are necessary to reach the state $g \approx g_{\text{guess}}$ if the first guess is well-chosen. Admittedly, slight discontinuities can arise during looping when the current density solution switches, for example, from the underdamped to the overdamped case due to an updated g_{guess}.

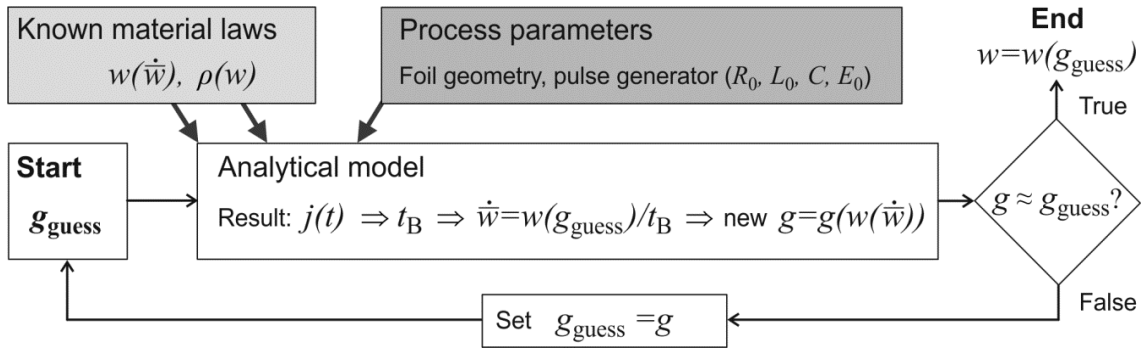

***Figure 5**: Flow chart of the solution scheme applied for the modeling*

4 Comparison between Experiments and Modeling

A representative comparison between experimental and modeling results of energy depositions, which shows both the strengths and the limits of the model, is displayed in **Fig. 6**. The experiments were partly repeated several times to check reproducibility, and did not follow a full factorial design. Most of the experiments were conducted on the comparatively faster SMU bank. With regard to **Eq. 7**, the actuator length must be changed to geometrically influence the foil resistance while maintaining V_a = const.. Note that there are many possibilities to adjust the cross section when the length is changed. Consequently, different thickness-width combinations (compare section **2.1**) having the same amount of area cannot be distinguished in **Fig. 6**.

In case of the slower pulse generator and the longest foils (**Fig. 6 a**), it can be seen that the experiments are in satisfying accordance with the modeling results (average deviation of 11%). However, recalling $j_{MHD} \approx (g - g_{melt}) \cdot \gamma^{-0.5}/12$ with $g_{melt} = 252 \cdot 10^6$ A^{2}s/cm^4 after Tucker and Toth (1975) and inserting experimental g-values, it becomes clear that the measured peak current densities $j_{peak} = I_{peak}/A$ of the shorter foils were below j_{MHD}, so that instabilities may have developed. If so, the simplifying assumption of uniform Joule heating is no longer valid, which means that the modeling results are not reliable in those cases.

Figs. 6 b-d show results for the SMU bank. In cases where $j_{peak}/j_{MHD} > 1$ applies (**Figs. 6 b-c**), the model is again in acceptable accordance with the experiments (average deviation: 15%). The higher the charging energy, the more energy can be deposited in roughly the same time ($t_B \approx 5$ µs here) as the capacitance remains unchanged. It can also be observed that the specific energy deposition increases when the foil length is decreased (at V_a = const.). Both assertions are supported by the modeling results.

It can further be stated that the model significantly underestimates the experiments for $j_{peak}/j_{MHD} < 1$, with a deviation of already about -40% at the border of its validity range ($j_{peak}/j_{MHD} \approx 1$, **Fig. 6 d**). Yet this magnitude of deviation is still in the range of the scattering of the experiment-based relation $w(\dot{\bar{w}})$ from **Fig. 3** which, in turn, is incorporated in the modeling as a kind of material law. Furthermore, a bigger data base for

the resistivity relation $\rho(w)$ would be beneficial as it is currently just based on very few values from literature.

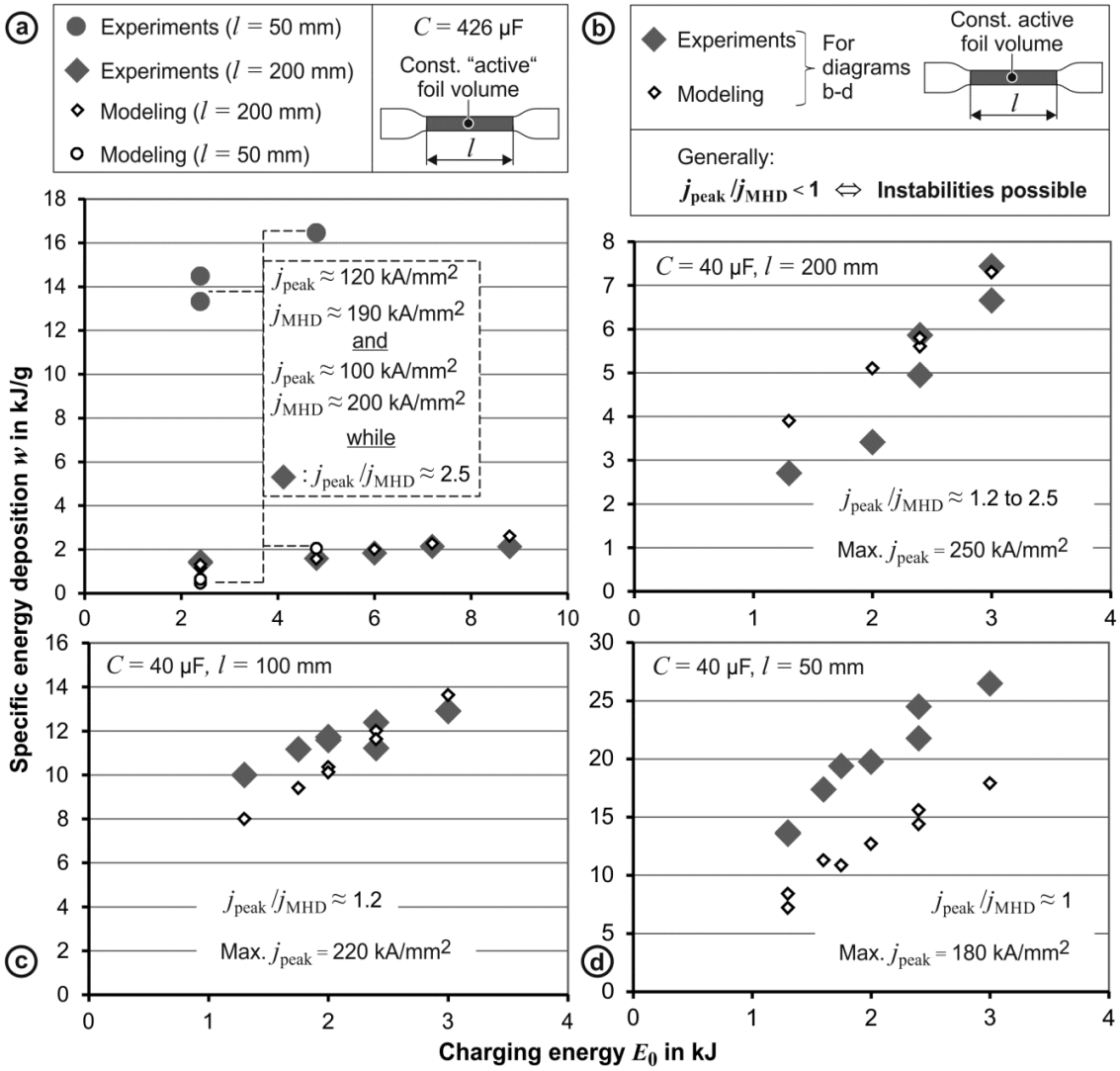

***Figure 6**: Result comparison: **a)** "Magneform", **b)-d)** "SMU0612"; $V_a = A \cdot l = 30.5\ mm^3$*

It is noticeable that the ratio between the total deposited energy and the initial charging energy ("pulse generator efficiency") was significantly higher for the SMU bank, also yielding higher heating rates and thus representing the region around $w/w_s \approx 2$ in **Fig. 3**. This is illustrated by the 200 mm long foil, for which a charging energy of 1.3 kJ on the SMU bank is enough to reach a higher energy deposition than with an 8.8 kJ shot on the Magneform bank. Accordingly, the region $w/w_s < 1$ in **Fig. 3** is mainly governed by experiments performed on the slower and less efficient Magneform bank. The modeling results confirm these findings, too.

5 Conclusion

The introduced model offers a quick first order approximation for the VFA process design, which correctly reflects the influences of the pulse generator configuration and the foil geometry on the energy output available for metalworking operations if uniform Joule heating is ensured. Future work will aim to improve the prediction accuracy of the model and to utilize it for VFA forming and welding applications.

Acknowledgements

This work was funded by the Deutsche Forschungsgemeinschaft DFG (German Research Foundation) in the frame of the project TE 508/69-1.

References

Al-Hassani, S.T.S., Can, M., Watson, E.J., 1986. A second order approximation to nonlinear circuit equations as applied to high energy electrical discharge processes. Journal of Computational and Applied Mathematics 15, pp. 175-189.

Hahn, M., Weddeling, C., Taber, G., Vivek, A., Daehn, G.S., Tekkaya, A.E., 2016. Vaporizing foil actuator welding as a competing technology to magnetic pulse welding. Journal of Materials Processing Technology 230, pp. 8-20.

Kazimierczuk, M.K., 2004. High-frequency magnetic components. Wiley, Chichester.

Osher, J.E., Barnes, G., Chau, H.H., Lee, R.S., Lee, C., Speer, R., Weingart, R.C., 1989. Operating characteristics and modelling of the LLNL 100-kV electric gun. IEEE Transactions on Plasma Science 17 (3), pp. 392-402.

Sedoi, V.S., Mesyats, G.A., Oreshkin, V.I., Valevich, V.V., Chemezova, L.I., 1999. The current density and the specific energy input in fast electrical explosion. IEEE Transactions on Plasma Science 27 (4), pp. 845-850.

Tkachenko, S.I., Vorob'ev, V.S., Malyshenko, S.P., 2004. The nucleation mechanism of wire explosion. Journal of Applied Physics D 37, pp. 495-500.

Tucker, T.J., Toth, R.P., 1975. A computer code for the prediction of the behavior of electrical circuits containing exploding wires. Report SAND 75-0041, Sandia Laboratories, Albuquerque, NM (USA).

Vivek, A., Taber, J.R., Johnson, J.R., Woodward, S.T., Daehn, G.S., 2013a. Electrically driven plasma via vaporization of metallic conductors: a tool for impulse metal working. Journal of Materials Processing Technology 213, pp. 1311-1326.

Vivek, A., Hansen, S.R., Liu, B.C., Daehn, G.S., 2013b. Vaporizing foil actuator: a tool for collision welding. Journal of Materials Processing Technology 213, pp. 2304-2311.

Weingart, R. C., Lee, R. S., Jackson, R. K., Parker, N. L., 1976. Acceleration of thin flyers by exploding foils: application to initiation studies. In: Proceedings of the 6th International Symposium on Detonation, Coronado CA, USA, pp. 653-663.

Winkler, R., 1973. Hochgeschwindigkeitsbearbeitung: Grundlagen und technische Anwendung elektrisch erzeugter Schockwellen und Impulsmagnetfelder. VEB Verlag Technik, Berlin (in German).

Zou, Y., He, B., Jiang, X., Wang, L., 2012. Relationships between bridge foil parameters and input pulse current. In: Proceedings of the 2012 International Symposium on Safety Science and Technology, Procedia Engineering 45, pp. 1020-1024.